

# Self-organized stochastic tipping in slow-fast dynamical systems

**Mathias Linkerhand, Claudius Gros**

Institute for Theoretical Physics, Goethe University, Frankfurt a. M., Germany

E-mail: linkerhand[at]th.physik.uni-frankfurt.de

E-mail: gros[at]th.physik.uni-frankfurt.de

**Abstract.** Polyhomeostatic adaption occurs when evolving systems try to achieve a target distribution function for certain dynamical parameters, a generalization of the notion of homeostasis. Here we consider a single rate encoding leaky integrator neuron model driven by white noise, adapting slowly its internal parameters, the threshold and the gain, in order to achieve a given target distribution for its time-average firing rate. For the case of sparse encoding, when the target firing-rate distribution is bimodal, we observe the occurrence of spontaneous quasi-periodic adaptive oscillations resulting from fast transition between two quasi-stationary attractors. We interpret this behavior as self-organized stochastic tipping, with noise driving the escape from the quasi-stationary attractors.

## 1. Introduction

Self-regulation plays an important role in biological and technical systems. Homeostatically regulated steady states are a precondition to life, examples being the concentration of blood glucose controlled by insulin [1] and glucagon, the pH value of blood [2, 3] and the body temperature [4], which are all autoregulated in order to maintain stable conditions. Further examples are the concentration of ions, proteins and transmitters in the brain, their respective levels are all self regulated [5]. Furthermore, homeostasis is implemented and can be found in technical systems, for example in microrobotic swarms [6]. Adaption typically introduces a slow time scale into the dynamical system [7], a process also denoted meta learning, a central notion in the context of neuromodulation [8] and emotional control [9]. The resulting dynamical system then has both fast and slow variables and critical transitions in the form of tipping processes may occur [10].

Classical homeostasis involves the regulation of a scalar quantity, like the body temperature. More complex forms of homeostasis are however also important in the realm of life. For example, an animal may want to achieve a certain time averaged distribution of behaviors, like foraging, resting and engaging socially, over the course of several days. This kind of adaptive behavior has been termed polyhomeostasis [11, 12]. It occurs when a dynamical system tries to achieve, via the continuous adaption of slow variables, a given target distribution for the time-averaged activity of a subset of fast variables. Polyhomeostatically adapting systems are typically slow-fast dynamical systems and their dynamical behavior can tip spontaneously from one state into another. For a network of rate-encoding neurons tipping transitions from laminar flow to intermittent chaotic bursts of activities have been observed [11, 12].

Tipping transitions can occur both in adaptive and in driven systems. Potential tipping scenarios are currently discussed intensively in the context of climate research [13, 14], they may be related to a slow driving of external parameters [15], to noisy input inducing a stochastic escape from a local attractor [16, 17], or through a dynamical effect when the rate of change of a control parameter reaches a certain threshold [13].

Here we study the phenomenon of self-organized tipping for a polyhomeostatic adapting system driven by a steady-state stochastic input. We examine a previously proposed model [18, 19] for regulating the firing rate distribution of individual neurons based on information-theoretical principles. This type of model has been studied previously for the case of discrete time systems and unimodal target firing rate distributions [11, 12]. Here we examine the case of continuous time and bimodal target distribution functions, corresponding to sparse coding. For bimodal firing rate distributions the neural activity tends to switch in between states close to minimal and maximal activity. Similar bimodal activity states are observed also in many other systems, e.g. dynamical gene regulation networks [20]. We find that bimodal target distributions may lead to self-organized bistability within a certain range of parameters.

We consider a single leaky integrator neuron with noisy input and a sigmoidal

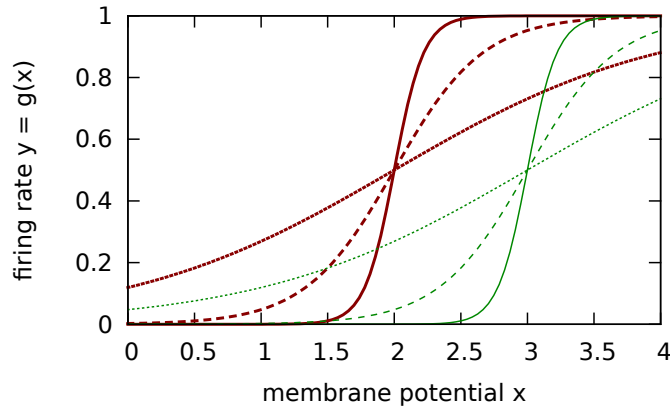


**Figure 1.** The transfer function  $g(x)$ , see Eq. (2), for thresholds  $b = 2$  (red lines) and  $b = 3$  (green lines) and various gains  $a$ : 1 (dotted), 3 (dashed), 9 (solid).

transfer function having two degrees of freedom. To achieve a special behavior – here the temporal output distribution of the firing rate – we use polyhomeostasis to change the intrinsic parameters which are directly influencing the mapping of the membrane potential to the firing rate in order to obtain a specific output distribution. We derive these parameter changing rules using stochastic adaption and show that two degrees of freedom already result in a good behavior approximation, for most of the parameters studied. For bimodal adaption target distributions we observe self-organized and quasi periodic stochastic tipping in between two quasi-stationary attractors resulting from competing adaption gradients.

## 2. Model

Biological neurons integrate incoming signals and emit an axon potential, a spike, whenever the membrane potential has reached a certain threshold. The membrane potential then returns, after a short refractory period, rapidly to its resting value. This behavior can be captured using spiking integrate and fire neural models [21]. In many circumstances the firing rate, the number of spikes per unit time, is important and rate encoding neural models can be used [22]. Here we consider a single rate-encoding leaky integrator driven by white noise  $\xi(t)$ ,

$$\dot{x}(t) = -\Gamma x(t) + \xi(t), \quad \langle \xi(t)\xi(t') \rangle = Q\delta(t - t'), \quad (1)$$

where  $x > 0$  is the membrane potential and  $\Gamma > 0$  the relaxation rate. The firing rate  $y(t) \in [0, 1]$  is a nonlinear function of the membrane potential  $x(t)$ , which we have selected as

$$y(t) = g(x(t)), \quad g(x) = \frac{1}{1 + e^{-a(x-b)}}, \quad (2)$$

where  $a > 0$  is the gain and  $b$  is the threshold. The polynomial transfer function (2) maps the membrane potential  $x \in [-\infty, \infty]$  to the normalized firing rate  $y \in [0, 1]$

which approaches zero and unity for small and large membrane potentials respectively, compare Fig. 1. The slope of  $g(x)$  is  $a/4$  at the threshold  $b$ .

Usually the intrinsic parameters of the transfer function (2),  $a$  and  $b$  are taken as given by some a priori considerations. Here we will consider them to be slow variables,  $a = a(t)$  and  $b = b(t)$ , adapting slowly such that a target dynamical behavior is approached on the average for the firing rate  $y(t)$ . The stochastic driving  $\xi(t) \in [\Xi_1, \Xi_2]$  in (1) is simulated through white noise plateaus: The values are generated according to a uniform probability distribution (white noise), but they remain constant for short time intervals on the order of unity. The membrane potential averages the input driving noise, due to the leak rate  $\Gamma$  in (1), its distribution function  $\rho(x)$  having a mean  $\mu_\rho \approx (\Xi_1 + \Xi_2)/(2\Gamma)$  and variance  $\sigma_\rho^2 \approx (\Xi_2 - \Xi_1)/(2\Gamma)$ .

### 2.1. Polyhomeostatic Adaption

The firing-rate statistics is given by

$$p(z) = \frac{1}{T} \int_{t_0}^{t_0+T} \delta(z - y(t)) dt, \quad \int_0^1 p(z) dz = 1, \quad (3)$$

where the length  $T$  of the sliding observation window is substantially larger than the relaxation rate  $1/\Gamma$ . The firing-rate distribution  $p(z)$  is an important quantity characterizing the information processing capability of biological and artificial neurons. No information is encoded for a constant firing rate, the next value is always exactly the same as before, so no new information is transferred. One may assume that a certain distribution  $q(y)$  of firing rates may constitute an optimal working regime. Possible functional dependencies for  $q(y)$  can be derived by information-theoretical considerations, e.g. maximizing information entropy, as discussed further below.

Considering a given target firing-rate distribution  $q(y)$ , the closeness of the actual firing-rate distribution  $p(y)$  is measured by the Kullback-Leibler divergence (KL-divergence)  $D_{\text{KL}}$ , their relative entropy, [7]:

$$D_{\text{KL}}(p, q) = \int dy p(y) \ln \frac{p(y)}{q(y)}, \quad D_{\text{KL}}(p, q) \geq 0. \quad (4)$$

The Kullback-Leibler divergence is positive definite and vanishes only when the two distribution coincide. The KL-divergence is generically not symmetric but becomes symmetric in the limiting case of similar distributions  $p$  and  $q$ , becoming equivalent in this limit to the  $\chi^2$  test [7]. Our aim is now to rewrite (4) as an integral over the membrane potential  $x$ , using

$$p(y)dy = \rho(x)dx, \quad p(y) = \frac{\rho(x)}{dy/dx}, \quad (5)$$

where  $\rho(x)$  is the membrane potential distribution. Using  $y = g(x)$  and Eqs. (4) and (5), we obtain

$$\frac{\partial D_{\text{KL}}}{\partial \theta} = \int dx \rho(x) \left[ -\frac{1}{g'} \frac{\partial g'}{\partial \theta} - \frac{q'}{q} \frac{\partial g}{\partial \theta} \right] \equiv \int dx \rho(x) \frac{\partial d}{\partial \theta} \quad (6)$$

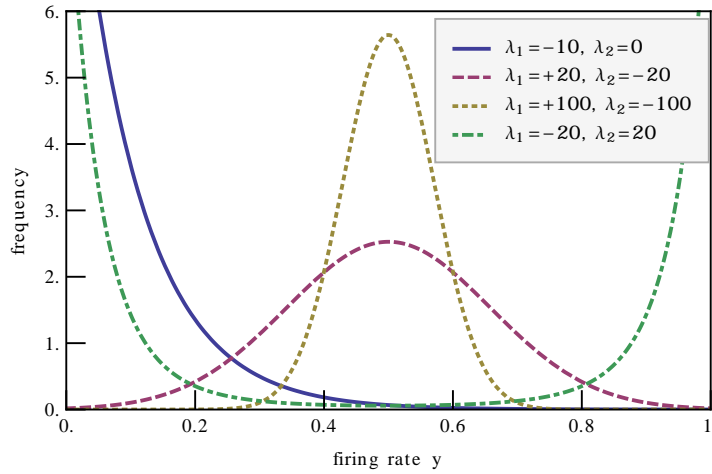


**Figure 2.** Target distribution  $q(y)$ , see (9), with some selected parameters  $\lambda_1$  and  $\lambda_2$ . The target firing-rate distributions is bimodal for  $\lambda_2 > 0$ .

for the derivative of the Kullback-Leibler divergence with respect to the intrinsic parameters  $\theta = a, b$  of the transfer function  $g(x)$ , see (2).

We consider now the case that the system does not dispose of prior information about the distribution of input stimuli and the thereby resulting distribution of membrane potential  $\rho(x)$ . The best strategy to minimize the Kullback-Leibler is then to minimize the individual terms of the integral (6) through the stochastic adaption rules [18, 11]

$$\frac{d\theta}{dt} = -\epsilon_\theta \frac{\partial d}{\partial \theta}, \quad \theta = a, b \quad (7)$$

for the intrinsic parameters of the transfer function  $g(x)$ , where the  $\epsilon_\theta$  are appropriate small adaption rates.

## 2.2. Target Firing-Rate Distribution

In order to evaluate (7), respectively Eq. (6), we need to specify the target firing rate distribution  $q(y)$ . For this purpose we use information-theoretical considerations.

Given a continuous probability distribution function  $q$  its Shannon entropy  $H(q)$  can be defined as

$$H(q) = - \int dy q(y) \ln q(y) \quad (8)$$

Among all the real-valued distributions with specified mean  $\mu$  and standard deviation  $\sigma$  the Gaussian distribution [7]

$$q(y) \propto \exp\left(-\frac{(y-\mu)^2}{2\sigma^2}\right) \propto \exp(\lambda_1 y + \lambda_2 y^2) \quad (9)$$

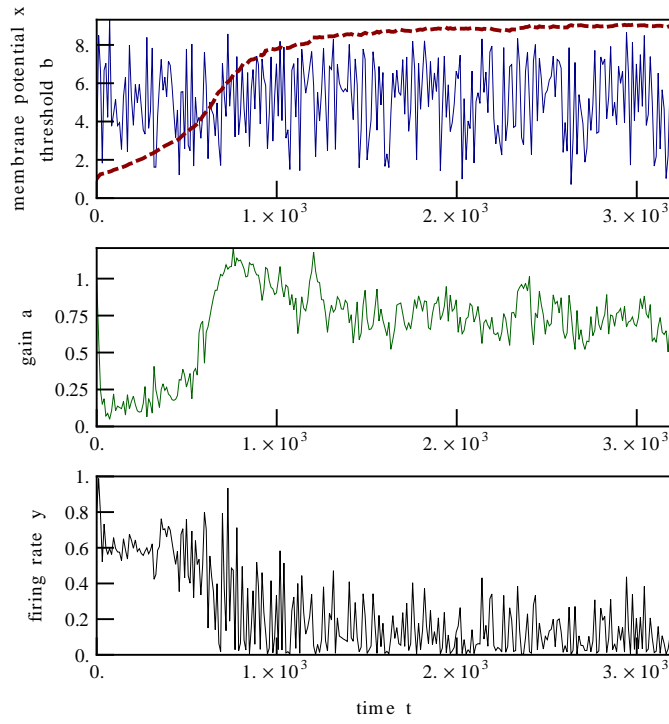


**Figure 3.** Typical time series for a mono-modal target distribution  $q(y)$  with  $\lambda_1 = -10$ ,  $\lambda_2 = 0$ , compare Fig. 2. Plotted are the membrane potential  $x$  (solid blue line, upper panel), the threshold  $b$  (dashed red line, upper panel), the gain  $a$  (solid green line, middle panel) and the firing rate  $y$  (solid black line, lower panel).  $\Delta t = 10^{-1}$ ,  $\epsilon_a = \epsilon_b = 10^{-2}$ ,  $\Gamma = 1$ .

has maximal information entropy, with  $\mu = -\lambda_1/(2\lambda_2)$  and  $2\sigma^2 = -1/\lambda_2$ , which is easily obtained using variational calculus,

$$0 = \delta \left[ H(q) + \lambda_1 \int dy y q(y) + \lambda_2 \int dy y^2 q(y) \right] ,$$

where  $(-\lambda_1)$  and  $(-\lambda_2)$  are the respective Lagrange parameters. In Fig. 2 examples for  $q(y)$  are illustrated for several values of  $\lambda_1$  and  $\lambda_2$ . The support of the target firing rates is compact,  $y \in [0, 1]$ , and both negative and positive  $\lambda_1$  and  $\lambda_2$  can be considered. The normalization factor  $\int_0^1 dy q(y)$  cancels out in (6), since only ratios are involved.

For positive  $\lambda_2 > 0$  and  $\lambda_1 \approx -\lambda_2$  one obtains bimodal target distributions. This is an interesting case, since sparse coding, which is realized when only a minority of neurons of a given network is active, and a majority is inactive [23], is characterized by a skewed bimodal distribution.

### 2.3. Stochastic Adaption Rules

From (9) and (2) we find the relations

$$\frac{q'(y)}{q(y)} = \lambda_1 + 2\lambda_2 y, \quad \frac{\partial g}{\partial x} = ag(1-g)$$

and

$$\frac{\partial g}{\partial a} = (x - b)g(1 - g), \quad \frac{\partial g}{\partial b} = -ag(1 - g),$$

which we can use to evaluate the stochastic adaption rules (7) as

$$\frac{da}{dt} = \epsilon_a \left[ \frac{1}{a} + (x - b) \left[ 1 - 2y + (\lambda_1 + 2\lambda_2 y)(1 - y)y \right] \right] \quad (10)$$

and

$$\frac{db}{dt} = \epsilon_b \left[ -a \left( 1 - 2y + (\lambda_1 + 2\lambda_2 y)(1 - y)y \right) \right]. \quad (11)$$

These two adaption rules will lead to an adaption of the time-averaged firing rate distribution  $p(y)$  towards the target distribution  $q(x)$  whenever the adaption time-scales  $1/\epsilon_\theta$  are substantially larger than the time constants of the neural dynamics, which in turn are determined by the time scale of the incoming stimuli and by the leak-rate  $\Gamma$  in (1).

The transfer function  $g(x)$  contains only two free parameters, the gain  $a$  and the threshold  $b$ . Perfect adaption  $p(y) \equiv q(y)$ , for all  $y \in [0, 1]$  can hence not be expected. The system tries to minimize the Kullback-Leibler divergence by adapting the available degrees of freedom, which are just two in our case.

#### 2.4. Numerical method

The equations (1), (10) and (11) form a set of first order differential equations with respect to time. We solve them numerically using the Euler method with one evaluation per time step. The random white noise is generated through a pseudo-random number generator with a uniform distribution. The values for the leak  $\Gamma$ , the time step  $\Delta t$  and the learning rates  $\epsilon_a$  and  $\epsilon_b$  are shown in the corresponding figures.

### 3. Results

We performed a series of simulations with the aim to study two issues. Polyhomeostatic adaption had been studied previously for the case of discrete time systems [18, 11], here we examine the case of continuous time. The case of a bimodal target distribution is, in addition, highly interesting, as it confronts the system with a dilemma. The transfer function  $g(x)$ , compare Fig. 1, is strictly monotonic. The distribution of the membrane potential  $\rho(x)$  is hence mono-modal. There is no easy way for the adapting neuron to achieve, as a steady state time-average, a bimodal output firing rate distribution  $p(y)$ . The question then is whether the system will find a way out of this dilemma through spontaneous behavioral changes.

#### 3.1. Target Distribution Approximation

For most simulations we used, if not stated otherwise,  $\Gamma = 1$  for the leak rate and  $\Delta t = 10^{-1}$  for the integration time step. A typical time series is given in Fig. 3. Note

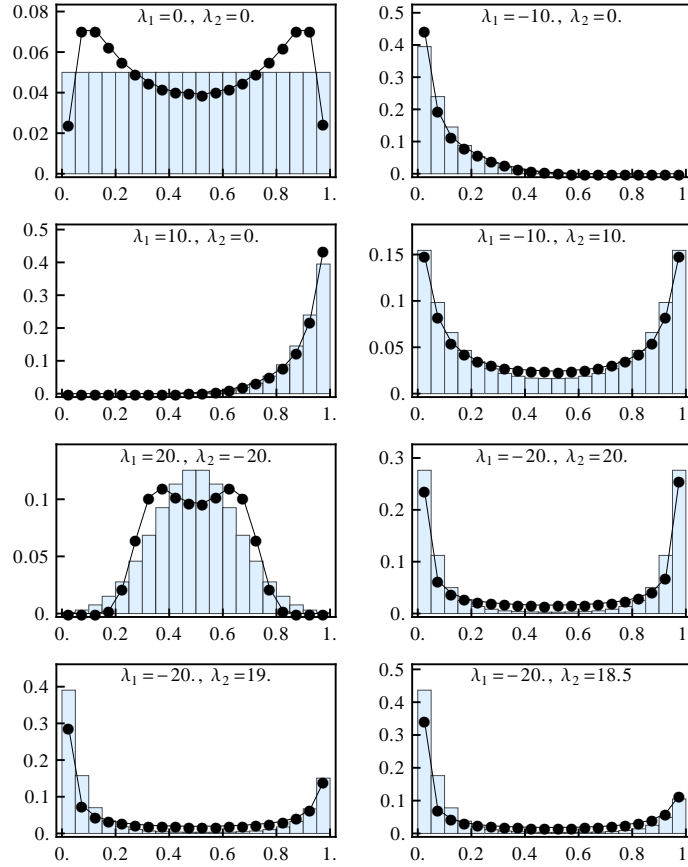


**Figure 4.** Target distribution  $q$  (bars) vs. achieved distribution  $p$  (points) for different distributions.  $\lambda_1$  and  $\lambda_2$  are given in each diagram.  $\Delta t = 10^{-1}$ ,  $t_{\max} = 10^8$ ,  $\epsilon_a = \epsilon_b = 10^{-2}$ ,  $\Gamma = 1$ ,  $\Xi = [0, 10]$ .

that the adaption of the intrinsic parameters  $a$  and  $b$  takes place on a slower time scale than the one of the primary dynamic variables,  $x$  and  $y$ , as typical for a slow-fast dynamical system.

Applying moderate to small learning rates  $\epsilon_a = \epsilon_b \lesssim 0.01$  the neuron's firing rate  $y$  approximates various types target distributions  $q$  quite well. In Fig. 4 the achieved and the respective target firing rate distributions are compared. The respective relative entropies are well minimized and presented in Table 1. Strictly speaking the stochastic adaption rules (10) and (11) are equivalent to approximating the firing-rate statistics (3), which is a time-averaged quantity, towards the target distribution function  $q(y)$  only in the limit of very small adaption rates,  $\epsilon_a$  and  $\epsilon_b$ . Small but finite values for the adaption rates, as used in our simulations, correspond to a trailing averaging procedure over a limited time interval, and the value of Kullback-Leibler divergence achieved hence depend weakly on the actual values used for the learning rates.

For very high learning rates,  $\epsilon_b \gg 0.1$ , the threshold  $b$  follows the membrane potential  $x$  nearly instantaneously, both variables become highly correlated. Therefore the firing rate distribution  $p$  cannot approximate the target distribution  $q$  any more, in



fact the resulting Kullback-Leibler divergence is then very high. The tipping in dynamic behavior as a function of adaption rate amplitude is typical for a rate-induced tipping transition [13].

### 3.2. Gain-Threshold Phase Diagram

Due to the sigmoidal shape of the transfer function, several target distributions lead to specific fingerprints in the gain-threshold phase diagram which we present in Fig. 5. The threshold, for example, for a left (right) dominant target distribution is high (low) and is therefore sensitive to the mean  $\mu = -\lambda_1/(2\lambda_2)$  of  $q(y)$ . Small gains  $a$  result in quite flat transfer functions  $g(x)$ , compare Fig. 1, mapping the membrane potentials to similar firing rates  $y$ . High gains  $a$  discriminate, relative to the threshold  $b$ , on the other side between high and low membrane potentials. The gain is therefore smaller for hill shaped and flat target distributions, as compared to the left and right dominant target distributions (e.g.  $\lambda_1 = -20$ ,  $\lambda_2 = +20$ ) for which intermediate values are suppressed.

Left (right) dominant target distributions (compare Table 1) correspond directly to high (low) transfer function thresholds. Uniform, hill and other not unilateral dominant target distributions lead to intermediate transfer function thresholds with a wide variety of the transfer function gains. For symmetrical target distributions from hill shaped to diametrical shaped there is a transition from low to high gains.

### 3.3. Self-Organized Stochastic Escape

While the left or right dominant target distributions are easily approximated due to the sigmoidal shape of the transfer function, the bimodal left and right dominant target distributions puts the system in dilemma: Since intermediate values are to be suppressed the transfer function gain  $a$  cannot be too small. Because of this there exists at least two quasi-stationary fixed points, one for the left, one for the right part of the distribution.

For zero or small learning rates  $\epsilon_a = \epsilon_b \approx 0$  the system is trapped in a single local fixed point. Only the left or right part of the target distribution is then approximated,

**Table 1.** The relative entropies  $D_{KL}$  (4) of various target distributions (see Fig. 2) compared to the corresponding achieved distribution, compare Fig. 4.

$\lambda_1$	$\lambda_2$	shape	$D_{KL}$
0	0	uniform	0.043
-10	0	left dominant	0.034
+10	0	right dominant	0.028
-10	+10	left/right dominant	0.018
+20	-20	hill	0.076
-20	+20	left/right, symmetric	0.175
-20	+19	left/right, left skewed	0.244
-20	+18.5	left/right, left skewed	0.283

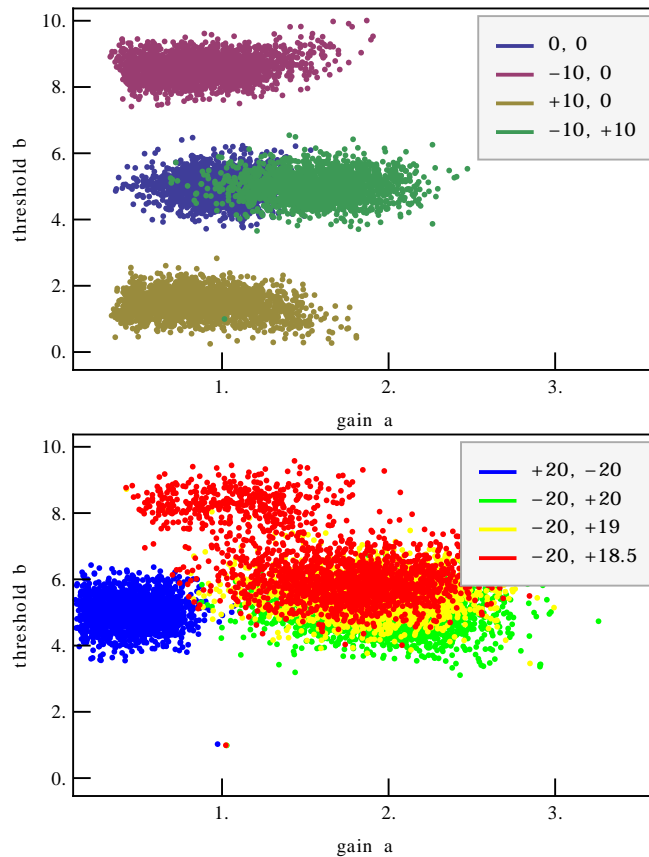


**Figure 5.** Phase diagram. Plotted are the gain  $a(t)$  and the threshold  $b(t)$  of the transfer function for various target distributions ( $\lambda_1$  and  $\lambda_2$  given in the legend). The respective target and achieved firing rate distributions are given in Fig. 4.

the Kullback-Leibler divergence is not well minimized.

Increasing the learning rates  $\epsilon_a = \epsilon_b$  allows the system to escape stochastically from the respective local fixed points: The transfer function threshold  $b$  conquers the local gradient and moves to the other fixed point and back (compare Fig. 6). In the long-term observation the system therefore approximates the left and the right part of the target distribution and hence minimizes the relative entropy, compare Table 2. These tipping transitions between the two quasi-stationary fixed points are illustrated in Fig. 7, which shows a typical time series for a skewed target distribution. Note that there are two fixed points for the gain and threshold and a direct correspondence to the periods of high and low firing rates  $y(t)$ .

**Table 2.** Relative entropies  $D_{KL}$  (4) for the left-skewed target distribution ( $\lambda_1 = -20$ ,  $\lambda_2 = 18.5$ ) relative to the achieved distribution for various learning rates  $\epsilon_a$  and  $\epsilon_b$ , compare Fig 6.

$\epsilon_a = \epsilon_b$	$10^{-5}$	$10^{-4}$	$10^{-3}$	$5 \cdot 10^{-3}$	$10^{-2}$	$5 \cdot 10^{-2}$	$10^{-1}$
$D_{KL}$	0.306	0.295	0.293	0.289	0.283	0.154	0.109

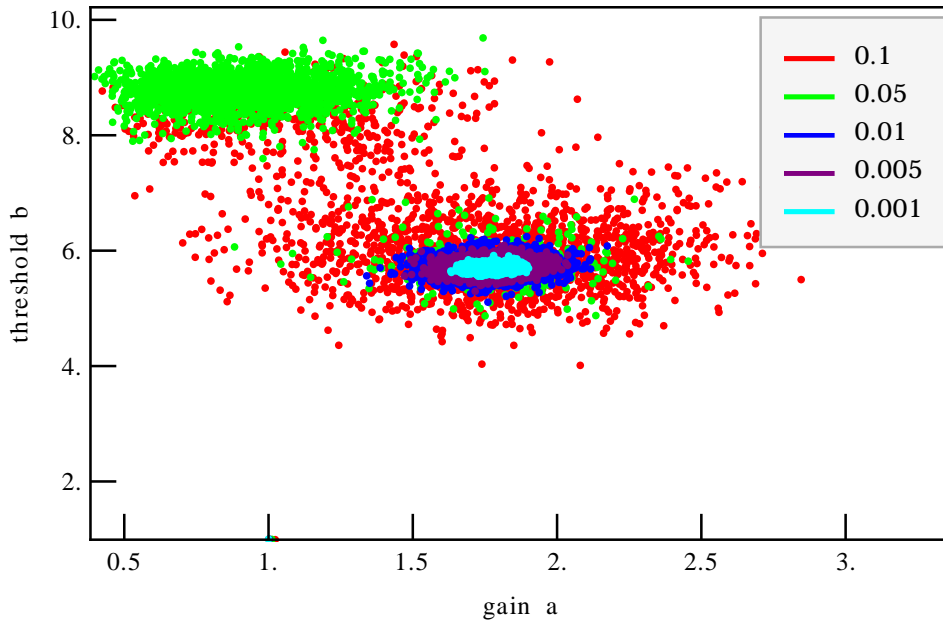


**Figure 6.** Stochastic escape: Phase diagram of the transfer function gain vs. transfer function threshold for a convex left skewed target distribution with various learning rates ( $\epsilon_a = \epsilon_b$  given in the legend).  $\Delta t = 10^{-1}$ ,  $\Gamma = 1$ ,  $\lambda_1 = -20$ ,  $\lambda_2 = 18.5$ .

Very low learning rates  $\epsilon_a$ ,  $\epsilon_b$ , lead to deep and big basins of attraction for the respective fixed points, while on the other hand high learning rates result in the closely following of the threshold to the membrane potential which prohibits reaching the target distribution. This mechanism is reminiscent to the case of Langevin dynamics in a double-well potential [24], where a stochastically driven particle may switch forth and back between two local minima [7]. The switching time is controlled for the double-well problem by the Kramer’s escape rate, which depends exponentially on the potential barrier height. It is difficult to formulate a quantitative mapping to the double-well problem, the local attractors visible in Figs. 6 and 7, and the effective barriers in between them, are self-organized structures. Note that the strength  $Q$  of the noise term (1) is constant and influences the transition rate only weakly, due to the continuous adaption of the transfer function, via (10) and (11), to the average strength of the stochastic driving.

#### 4. Discussion

We showed that polyhomeostatic adaption of continuous-time leaky integrator leads to desired firing rate distributions. We also run further simulations using white noise and Gaussian noise input and replace the transfer function by other qualitatively different (but still sigmoidal) functions, see Appendix. It turns out that the polyhomeostatic adaption as well as the self-organized stochastic escape are quite robust principles. However, the quality of the approximation (as seen by visual overlapping) and the value of the Kullback-Leibler divergence depend on the learnings rates, but also on the

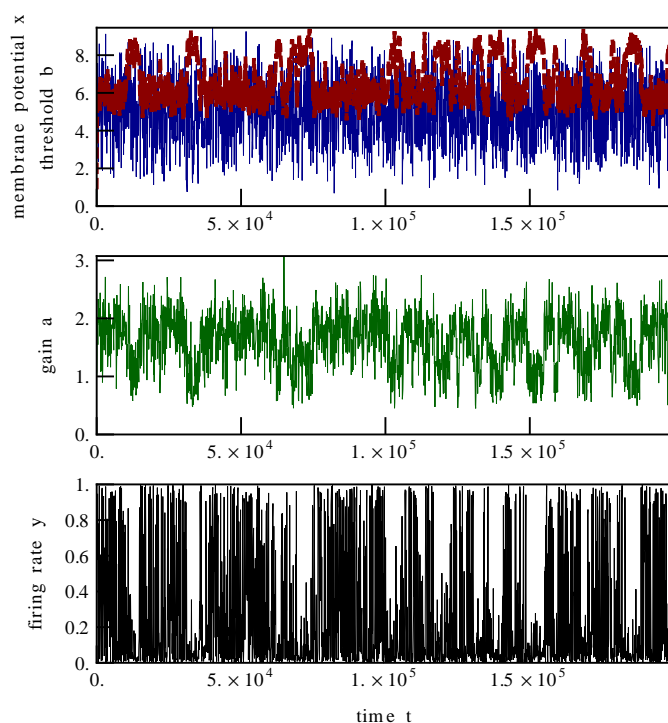


**Figure 7.** Time series: membrane potential  $x$ , transfer function threshold  $b$  (dashed), transfer function gain  $a$  and firing rate  $y$ .  $\Delta t = 10^{-1}$ ,  $\epsilon_a = \epsilon_b = 10^{-1}$ ,  $\Gamma = 1$ ,  $\lambda_1 = -20$ ,  $\lambda_2 = 18.5$ .

input distribution and the input's strength.

The stochastic tipping as a function of adaption rates has a close relation to the phenomenon of stochastic escape. The strength of the driving input noise is constant, but its influence is averaged out for very low adaption rates. Stochastic escape from one local attractor to another is not possible. The stochasticity of the input becomes relevant for intermediate values of adaption rates and stochastic transitions between the two quasistationary attractors are most frequent. Finally, for very large adaption rates, the system tips into another dynamical state, tracking the stochastic input signal nearly instantaneously. This sequence of behaviors is self organized and reached from any initial state.

## References

- [1] L. Plum, B.F. Belgardt, J.C. Brüning, *The Journal of Clinical Investigation* **116**, 1761–1766 (2006).
- [2] E.K. Schaefer, Blood ph and pCO<sub>2</sub> homeostatis in chronic respiratory acidosis related to the use of amine and other buffers, *Annals of the New York Academy of Sciences* **92**, 401–413 (1961).
- [3] M. Tresguerres, S.K. Parks, E. Salazar, L.R. Levin, G.G. Goss, J. Buck, Bicarbonate-sensing soluble adenylyl cyclase is an essential sensor for acid/base homeostasis *Proceedings of the National Academy of Sciences* **107**, 442–447 (2010).
- [4] N. Charkoudian, Skin blood flow in adult human thermoregulation: how it works, when it does not, and why, *Mayo Clinic Proceedings* **78**, 603–612 (2003).

- [5] E. Marder, and J.M. Goaillard, Variability, compensation and homeostasis in neuron and network function, *Nature Reviews Neuroscience* **7**, 563 (2006).
- [6] S. Kernbach, O. Kernbach, Collective energy homeostasis in a large-scale microrobotic swarm, *Robotics and Autonomous Systems* **59**, 1090–1101 (2011).
- [7] C. Gros, *Complex and Adaptive Dynamical Systems, A Primer*, Springer (2008); second edition 2010.
- [8] K. Doya, Metalearning and neuromodulation, *Neural Networks* **15**, 495–506 (2002).
- [9] C. Gros, Cognition and Emotion: Perspectives of a Closing Gap *Cognitive Computation* **2**, 78 (2010).
- [10] C. Kuehn, A mathematical framework for critical transitions: bifurcations, fast-slow systems and stochastic dynamics, *Physica D: Nonlinear Phenomena* **240**, 1020–1035 (2011).
- [11] D. Markovic, C. Gros, Self-organized chaos through polyhomeostatic optimization, *Physical Review Letters* **105**, 068702 (2010).
- [12] D. Markovic, C. Gros, Intrinsic Adaption in Autonomous Recurrent Neural Networks, *Neural Computation* **24**, 523 (2012).
- [13] P. Ashwin, S. Wiczorek, R. Vitolo, P. Cox, Tipping points in open systems: bifurcation, noise-induced and rate-dependent examples in the climate system *Phil. Trans. R. Soc. A* **370** 1166-1184 (2012).
- [14] T.M. Lenton, H. Held, E. Kriegler, J.W. Hall, W. Lucht, S. Rahmstorf, H.J. Schellnhuber, Tipping elements in the Earth's climate system, *Proceedings of the National Academy of Sciences* **105**, 1786 (2008).
- [15] S.M. Baer, T. Erneux, J. Rinzel, The slow passage through a Hopf bifurcation: delay, memory effects, and resonance, *SIAM Journal on Applied mathematics* **49**, 55–71 (1989).
- [16] L. Gammaitoni, P. Hänggi, P. Jung, F. Marchesoni, Stochastic resonance, *Reviews of Modern Physics* **70**, 223 (1998).
- [17] M.D. McDonnell, D. Abbott, What is stochastic resonance? Definitions, misconceptions, debates, and its relevance to biology, *PLoS computational biology* **5**, e1000348 (2009).
- [18] J. Triesch, A gradient rule for the plasticity of a neuron's intrinsic excitability, in *Proceedings of ICANN 2005*, W. Duch et al. (Eds.), LNCS **3696**, 65 (2005).
- [19] M. Stemmler, C. Koch, How voltage-dependent conductances can adapt to maximize the information encoded by neuronal firing rate, *Nature Neuroscience* **2**, 521 (1999).
- [20] E.H. Davidson, D.H. Erwin, Gene regulatory networks and the evolution of animal body plans. *Science* **311**, 796 (2006).
- [21] A.N. Burkitt, A review of the integrate-and-fire neuron model: I. Homogeneous synaptic input, *Biological cybernetics* **95**, 1–19 (2006).
- [22] A. Borst, F.E. Theunissen, Information theory and neural coding, *Nature Neuroscience* **2**, 947–958 (1999).
- [23] B.A. Olshausen, and D.J. Field, Sparse coding of sensory inputs, *Current opinion in neurobiology* **14**, 481–487 (2004).
- [24] P. Hanggi, Escape from a metastable state, *Journal of Statistical Physics* **42**, 105 (1986).

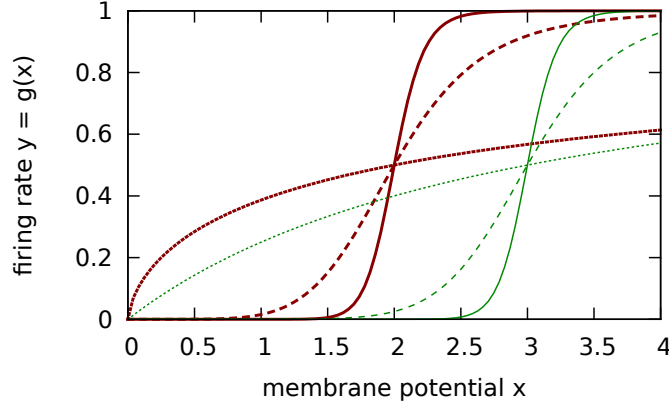


**Figure A1.** The transfer function  $g(x)$ , see Eq. (A.1), for thresholds  $b = 2$  (red lines) and  $b = 3$  (green lines) and various gains  $a$ :  $1/3$  (dotted),  $3$  (dashed),  $9$  (solid). No inflection point is present for exponents  $ab < 1$ .

## Appendix A. Polynomial transfer function

The polyhomeostatic adaption of the system is not changing qualitatively by replacing the transfer function  $g$ . Instead it turns out that the system is robust against changing the transfer function as long as it remains sigmoidal. We also applied a transfer function

$$g(x) = \frac{(x/b)^{ab}}{(x/b)^{ab} + 1}, \quad (\text{A.1})$$

with a polynomial decay to  $g(0) = 0$ , which limits the membrane potential  $x \geq 0$  to be non-negative. It turns out that the shape of the target distribution  $q$  is also well approximated using this transfer function. Also stochastic escape from one fixed point to another and back can be observed as for some target distributions two fixed points are necessary.

The transfer function has an inflection point for exponents  $ab > 0$ ; it is absent for  $ab < 1$ , compare Fig. A1. The transfer function  $g$  behaves as

$$g(x) \approx \begin{cases} (x/b)^{ab} & x \ll b \\ \frac{1}{2} + \frac{1}{4}a(x-b) & x \approx b \\ 1 - (b/x)^{ab} & x \gg b \end{cases}. \quad (\text{A.2})$$

The slope is  $a/4$  which approaches zero and unity for small and large membrane potentials respectively.

From Eq. (A.1) we find the relations

$$\frac{\partial g}{\partial x} = (1-g)g \frac{ab}{x}, \quad (\text{A.3})$$

$$\frac{\partial g}{\partial a} = (1-g)gb \ln\left(\frac{x}{b}\right), \quad \frac{\partial g}{\partial b} = (1-g)ga \left[ \ln\left(\frac{x}{b}\right) - 1 \right], \quad (\text{A.4})$$

which we can use to evaluate the stochastic adaption rules (7) as

$$\frac{da}{dt} = \epsilon_a \left[ \frac{1}{a} - b \ln(x/b) \left[ 1 - 2y + (\lambda_1 + 2\lambda_2 y)(1-y)y \right] \right] \quad (\text{A.5})$$

and

$$\frac{db}{dt} = \epsilon_b \left[ \frac{1}{b} - a \left[ \ln(x/b) - 1 \right] \left[ 1 - 2y + (\lambda_1 + 2\lambda_2 y)(1 - y)y \right] \right]. \quad (\text{A.6})$$

Applying this transfer function  $g$  it turns out that the target distribution is well approximated also in this case, even though the membrane potential is restricted to non-negative numbers. Tab. A1 lists the well minimized Kullback-Leibler divergences for several target distributions.

We conclude that the stochastic adaption rules are therefore generic and qualitatively independent on the concrete realization of the transfer function. However, quantitatively the resulting relative entropies depend on the choice of the transfer function which also influences the optimal adaption rates  $\epsilon_a$  and  $\epsilon_b$ .

### Appendix A.1. Self-Organized Stochastic Escape

For the non-symmetric convex target distribution ( $\lambda_1 = -20$ ,  $\lambda_2 = 19$ ) there are two fixed points. Since the target distribution cannot be well approximated by only one fixed point the system escapes stochastically from one to the other and back with a certain period, compare Fig. A2. For small learning rates  $\epsilon_a = \epsilon_b \lesssim 0.01$  the system is trapped in only one fixed point. The relative entropy therefore is not well minimized.

For intermediate learning rates  $0.01 \lesssim \epsilon_a = \epsilon_b \lesssim 0.04$  the perturbation is high enough to stochastically escape from that fixed point and approach another one. Fig. A2

**Table A1.** Relative entropies of various target distributions compared to the corresponding achieved distribution ( $\epsilon_a = \epsilon_b = 10^{-2}$ , bins = 100).

$\lambda_1$	$\lambda_2$	shape	$D_{KL}$
0	0	uniform	0.060131
-10	0	left dominant	0.069351
+10	0	right dominant	0.114578
-10	+10	left/right dominant	0.051811
+20	-20	hill	0.148098
-20	+20	left/right, symmetric	0.189217
-20	+19	left/right, left skewed	0.063934
-20	+18.5	left/right, left skewed	0.261215

**Table A2.** Relative entropies of the left-skewed target distribution ( $\lambda_1 = -20$ ,  $\lambda_2 = 19$ ) compared to the achieved distribution for various learning rates  $\epsilon_a$  and  $\epsilon_b$ . Note that the Kullback-Leibler divergence is not minimized for  $\epsilon_b \gtrsim 0.05$  due to the fast correlation of the membrane potential and the transfer function threshold.

$\epsilon_a = \epsilon_b$	$10^{-4}$	$10^{-3}$	0.01	0.03	0.04	0.05	0.06
$D_{KL}$	0.376	0.368	0.064	0.043	0.017	1.892	1.591

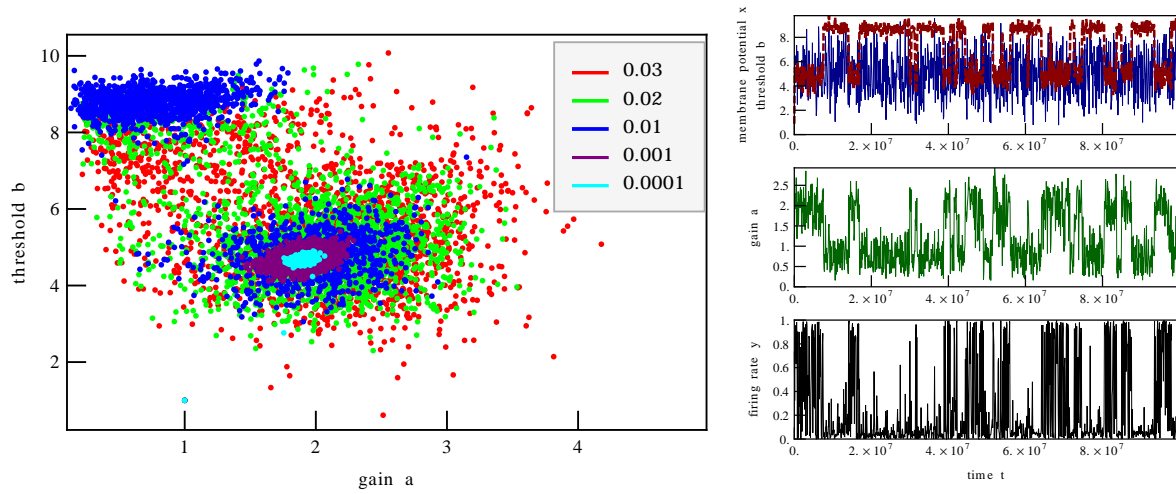


**Figure A2.** Left: Stochastic escape: Phase diagram of the transfer function gain vs. transfer function threshold for a convex left skewed target distribution with various learning rates ( $\epsilon_a$  and  $\epsilon_b$  given in the legend).  $\Delta t = 10^{-2}$ ,  $\Gamma = 0.1$ ,  $\lambda_1 = -20$ ,  $\lambda_2 = 19$ . Right: Time series: membrane potential  $x$ , transfer function threshold  $b$  (dashed), transfer function gain  $a$  and firing rate  $y$ .  $\Delta t = 10^{-1}$ ,  $\epsilon_a = \epsilon_b = 10^{-2}$ ,  $\Gamma = 0.1$ ,  $\lambda_1 = -20$ ,  $\lambda_2 = 19$ .

shows a typical time series for this tipping. This has also an effect on the relative entropy which therefore is even smaller than without stochastic escape (see Tab. A2).

For high learning rates  $\epsilon_a = \epsilon_b \gtrsim 0.05$  the system's behavior changes: the transfer function is close to a Heaviside step function and the threshold follows the membrane potential quickly. In that state the achieved distribution is not close to the target distribution, therefore the relative entropy is not minimized anymore (see Tab. A2).